Biomedicine & Pharmacotherapy 157 (2023) 114048

Contents lists available at ScienceDirect

Biomedicine & Pharmacotherapy

journal homepage: www.elsevier.com/locate/biopha

Melatonin inhibits ferroptosis and delays age-related cataract by regulating SIRT6/p-Nrf2/GPX4 and SIRT6/NCOA4/FTH1 pathways

Yu Mi [a,b,c,1], Chaoqun Wei [a,b,c,2], Liyao Sun [a], Huirui Liu [a,b,c], Jiayue Zhang [a,b,c], Jialin Luo [a], Xiaohan Yu [a], Jie He [a], Hongyan Ge [a,*], Ping Liu [a,*]

[a] Eye Hospital, First Affiliated Hospital, Harbin Medical University, 23 Youzheng Street, Harbin 150001, China
[b] Key Laboratory of Ischemia-reperfusion, Harbin Medical University, Ministry of Education, Harbin 150001, China
[c] Experimental Animal Centre, the Second Affiliated Hospital, Harbin Medical University, Harbin 150001, China

ARTICLE INFO

Keywords:
Ultraviolet B
Ferroptosis
Cataract
Melatonin
SIRT6

SUMMARY

Background: Cataracts are the main cause of reversible blindness worldwide. The ageing of the lens caused by ultraviolet B (UVB) radiation is mostly related to oxidative stress (OS). Little is known about whether OS induced by UVB enhances the sensitivity of lens epithelial cells to ferroptotic stress, which may be a new mechanism leading to age-related cataracts (ARCs).

Methods: Ferroptosis was detected by transmission electron microscopy (TEM), iron assay, lipid peroxidation (MDA) assay, real-time PCR, western blotting, and immunofluorescence. Genetic engineering technology was used to investigate the regulatory relationship among Sirtuin 6 (SIRT6), nuclear factor erythroid 2-related factor 2 (Nrf2), nuclear receptor coactivator 4 (NCOA4), glutathione peroxidase 4 (GPX4) and ferritin heavy chain (FTH1). Knockdown and overexpression of SIRT6 locally in vivo in rats were performed to probe the regulatory mechanism of SIRT6 in ferroptosis in ARCs.

Findings: Here, we observed that UVB can drastically induce ferroptosis in lens epithelial cells in vivo and in vitro. Surprisingly, inhibition of ferroptosis was the direct reason that melatonin rescued B-3, SRA01/04 and HEK-293 T cells survival; the pan-caspase inhibitor Z-Vad-FMK did not significantly reverse the death of UVB-irradiated cells compared with that in the UVB+DMSO group. SIRT6 was an upstream regulator of phosphorylated Nrf2 (p-Nrf2) and NCOA4 in B-3, SRA01/04 and HEK-293 T cells. Melatonin inhibited ferroptosis through the SIRT6/p-Nrf2/GPX4 and SIRT6/COA4/FTH1 pathways to neutralize lipid peroxidation toxicity, which protected cells against ferroptotic stress in vitro and delayed cataract formation caused by UVB exposure in rats.

Interpretation: Our findings reveal a novel causal role of melatonin in the pathogenesis of ARCs, which raises the possibility of selectively targeting the activation of SIRT6 and ferroptotic resistance as a latent antioxidative therapeutic strategy for ARCs.

1. Introduction

Cataracts are the primary cause of preventable blindness globally. With the ageing of the world's population, the proportion of age-related cataract (ARC) patients will increase in both developed and developing countries [1]. Surgical treatment of cataracts is the most effective method in the clinic. However, there is also a risk of intraoperative and postoperative complications, such as posterior capsule opacification, intraocular inflammation and corneal edema [2]. Among many kinds of environmental stresses, such as ultraviolet (UV) radiation, diabetes, drug intake, and excessive smoking and alcohol consumption, UV radiation is the most important risk factor for ARCs [3]. It has been shown that cortical and posterior subcapsular cataracts can be caused dose-dependently by consistent ocular ultraviolet B (UVB) radiation exposure [4]. The formation of cataracts induced by UVB begins with cumulative oxidative damage to human lens epithelial cells (HLECs) [5]. During this process, the modes of cell death include apoptosis [6], necroptosis [7] and pyroptosis [8].

* Corresponding authors.
E-mail addresses: gehongyan@hrbmu.edu.cn (H. Ge), liuping@hrbmu.edu.cn (P. Liu).
[1] First Author
[2] Co-First Author

https://doi.org/10.1016/j.biopha.2022.114048
Received 15 September 2022; Received in revised form 21 November 2022; Accepted 25 November 2022
Available online 1 December 2022

Table 1
Primary detailed grouping and the purposes of grouping in vitro.

Process	Grouping	Purpose of grouping
PartI	Control, UVB (0, 100, 200, 500, 750 and 1000 J/m^2)	To confirm the appropriate UVB irradiation range
PartII	Control, UVB (0, 100, 200 and 500 J/m^2)	To investigate the relationship between UVB-induced cell death and ferroptosis in the appropriate UVB range
PartIII	UVB+Control, UVB+DMSO, UVB+Fer-1,UVB+MT (50,100,250 μm)	To validate ferroptosis pathway and study the effect of dose-dependent MT on anti-ferroptosis
PartIV	DMSO, UVB+DMSO, UVB+MT, UVB+Z-VAD-FMK, UVB+Z-VAD-FMK+MT	To confirm the relationship between ferroptosis and apoptosis MT acted on.
PartV	DMSO, MT, UVB+DMSO, UVB+MT	To observe the effect of MT on cells with or without UVB irradiation
PartVI	UVB+MT+Control, UVB+MT+si-SIRT6(or si-Control)	To investigate the specific target protein (SIRT6) of MT inhibiting UVB-induced ferroptosis
PartVII	Control, UVB+Control, UVB+OE-SIRT6(or OE-Control), UVB+si-SIRT6(or si-Control)	To investigate the effect of differential expression of SIRT6 on UVB-induced ferroptosis
PartVIII	Control, OE-Nrf2(or OE-NCOA4), si-Nrf2(or si-NCOA4)	To determine the regulation between upstream and downstream of Nrf2(or NCOA4) with or without ferroptotic stress
PartIX	Erastin+Control,Erastin+OE-Nrf2(or OE-NCOA4),Erastin+si-Nrf2(or si-NCOA4)	

Table 2
Sequences of the siRNAs used in the experiments.

Primer	Species	Nucleotide sequence (5′−3′)
SIRT6	Human	Sense -GGUCAUUGUCAACCUGCAA- Antisense -CCAGUAACAGUUGGACGUU-
Sirt6	Rat	Sense -GCAUCUCAAUGGUUCCUAU- Antisense -CGUAGAGUUACCAAGGAUA-
NFE2L2	Human	Sense -UUGGGAUUCACGCAUAGGAGCACUG- Antisense -CAGUGCUCCUAUGCGGAAUCCCAA-
NCOA4	Human	Sense -GCUGUUUCUCUCAGUCAAUTT- Antisense -AUUCACUGAGAGAAACAGCTT-
Negative control	Human	Sense -UUCUCCGAACGUGUCACGUTT- Antisense -ACGUGACACGUUCGGAGAATT-
(NC)	Rat	Sense -GCUUUACUCUCUAUCAGGAUGAGAU- Antisense -AUCUCAUCCUGAUAGAGAGUAAAGC-

All siRNAs for rats were custom-designed for in vivo purity

Table 3
Primers for plasmid DNA used in the experiments.

Primer	Species	Nucleotide sequence (5′−3′)
SIRT6	Human	F-GGACAAGCTGGCCGAGCTGTACGGAAACAT- R-ACAGCTCGGCCAGCTTGTCCCTGGGGA-
Sirt6	Rat	F-GAGCGGAAGGTGTGGGAACT- R-TGAAGTCGGGGATGCCAGAGG-
NFE2L2	Human	F-ACACGGTCCACAGCTCATC- R-TGTCAATCAAATCCATGTCCTG-
NCOA4	Human	F-CTTTGGGCCGTAGGTTAGTG- R-GTTCTCTATTACTGGAGCTGCC-
Negative control	Human	F-AACTTTGGCATTGTGGAAGG- R-CACATTGGGGGTAGGAACAC-
(NC)	Rat	F-GGCTCCATGAACGGTGGTGTG- R-GCTGGTAGAGGAGTGTGCTTGC-

F, forward primer; R, reverse primer

Ferroptosis is an iron-dependent form of programmed cell death with unique triggering factors, regulatory factors and effectors [9]. The essence of ferroptosis is depletion of cysteine, which leads to deficit of reduced glutathione (GSH), toxic lipid alkoxy radicals in free iron-mediated Fenton-type reactions that disrupt the balance of the intracellular redox state, resulting in oxidative stress and lipid peroxidation both in the cell plasma membrane and in membranes of other internal organelles, triggering cell death [10].

Ferroptosis is now known to play a key role in the progression of neurodegenerative disorders, angiocardiopathy, cancer, and digestive diseases [11–13]. However, the role of ferroptosis in ARCs is still unclear. To date, a study has shown that there might be high sensitivity to ferroptosis among ageing FHL124 cells at approximately 55 passages treated with a low dose of the ferroptosis activator erastin and the glutathione peroxidase 4 (GPX4) inhibitor RSL3. These findings show that ferroptosis may play a crucial role in the etiology of ARCs [14].

Sirtuin 6 (SIRT6), a member of the sirtuin family, is a chromatin regulatory protein that has established roles in chromatin signaling and genome maintenance to postpone ageing and disease progression [15,16]. However, SIRT6 also plays a role in combating oxidative stress [17–19]. Recent studies have shown that SIRT6's prominent role in the survival of organisms is reflected in the downstream Nrf2/Keap-1/ARE antioxidant pathway [20–22]. Inhibition of miR4532 protects HLECs from UV-induced oxidative damage via activation of the SIRT6-Nrf2 pathway [23]. However, the effect of UVB radiation, a highly toxic oxidative stress generator, on SIRT6 and its downstream regulation are completely unknown.

Melatonin (MT), an amphiphilic tryptophan-derived indolamine, was first found in the pineal gland but soon detected almost everywhere in the mammalian body, and the amount produced elsewhere is approximately twice as much as that produced in the pineal gland [24–26]. MT acts as the circadian pacemaker of the central system and the biological clock of the peripheral organs. MT is also a highly potent free radical scavenger that is highly concentrated in mitochondria, regulates the activity of respiratory chain complexes I and IV [27], and protects mitochondrial DNA from mutations and deletions, showing significant immune regulation and antioxidant activity [28]. Our previous study confirmed that MT pretreatment of human lens epithelial cell lines can significantly inhibit H_2O_2-induced apoptosis and intracellular ROS production through the PI3K/Akt antiapoptotic signaling pathway and indicated that MT may have a potential therapeutic role in the prevention of ARCs [12].

In this study that was conducted based on our previous research, we discovered and used an unbiased method to study in depth the detailed protective mechanism of MT against ferroptosis and to explore the effect of MT on delaying the formation of age-related cataracts in vivo and in vitro. The findings are of great significance for further understanding the medicinal value of MT in the field of cataract treatment.

2. Materials and methods

2.1. Materials

Human lens epithelial cell line B-3 (B-3) was obtained from the American Type Culture Collection (ATCC Cat# CRL-11421, RRID: CVCL_6367), SRA01/04 and human embryonic kidney 293 T cell line (HEK-293 T) were purchased from Chinese Academy of Sciences (Shanghai, China). Foetal bovine serum (FBS) was purchased from Gibco (Thermo Fisher Scientific, Inc., Waltham, MA, USA), and Dulbecco's modified Eagle's medium was obtained from VivaCell Shanghai (Shanghai, China). UVB exposure was executed with a UVB radiometer (LUYOR-LEB-280 L, USA) with a total output of 5 W/m^2 (312 nm). A lux meter was used to test the irradiance of UV radiation. A Cell Counting Kit-8 (CCK-8) was purchased from Merck (Darmstadt, Germany). TRIzol and primers were obtained from Invitrogen (Eugene, Oregon, USA). Primary antibodies and fluorochrome-labeled secondary antibodies were purchased from Abcam (Cambridge, UK) and Proteintech (Chicago, IL, USA). All small molecular inhibitors and activators were obtained from MedChemExpress (Monmouth Junction, NJ, USA) and Cayman Chemical Company (Ann Arbor, MI, USA).

Table 4
Primers used for RT—PCR.

Primer	Nucleotide sequence (5′–3′)
GPX4	F-CGATACGCTGAGTGTGGTTT- R-CGGCGAACTCTTTGATCTCTT-
FTH1	F-TACCTGAATGAGCAGGTGAAAG- R-GATATTCCGCCAAGCCAGAT-
SLC7A11	F-GGTTGCCCTTTCCCTCTATTC- R-CCTGGGTTTCTTGTCCCATATAA-
SIRT6	F-CCCACGGAGTCTGGACCAT- R-CTCTGCCAGTTTGTCCCTG-
GAPDH	F-CTGGGCTACACTGAGCACC- R-AAGTGGTCGTTGAGGGCAATG-
LMNB1	F-TAGAGGAAAGCGGAAGAGGGTT- R-CCAGATGAGGTCAGTTGGGGGG-

F, forward primer; R, reverse primer

2.2. Methods

2.2.1. Cell culture and transfection

Cells were cultured in Dulbecco's modified Eagle's medium supplemented with 15% FBS at 37 °C in a humidified atmosphere with 5% CO_2. Cells were seeded for experiments when they reached the logarithmic growth phase and 70% confluence. The primary detailed grouping and the purposes of grouping in vitro experiments are summarized in Table 1.

Small interfering RNAs (siRNAs) or overexpression plasmids targeting SIRT6, nuclear factor erythroid 2-related factor 2 (Nrf2) and nuclear receptor coactivator 4 (NCOA4) were designed and synthesized by GenePharma (Shanghai, China). Three different siRNA or overexpression plasmid sequences for SIRT6, Nrf2 and NCOA4 were compared, and the one with the highest knockdown or overexpression efficiency (>80%) was chosen in the current study. All the detailed sequence information is summarized in Table 2 and Table 3. B-3, SRA01/04 or HEK-293 T cells were transfected with plasmid DNA (4 μg) or siRNA (100 pM) via Lipofectamine™ 2000 (Invitrogen, Carlsbad, CA, USA). After transfection for 48 h, cell lysates were harvested for further experiments.

2.2.2. Animals

Six-week-old albino Sprague—Dawley (SD) male rats were provided by the Experimental Animal Centre of the Second Affiliated Hospital of Harbin Medical University. The rats were reared in cages with four rats per cage and allowed to freely drink water and eat pelleted commercial food.

Ethical approval was obtained from the First Affiliated Hospital, Harbin Medical University. All animal experiments and treatments adhered to the guidelines in the Association for Research in Vision and Ophthalmology Statement for the Use of Animals in Ophthalmic and Vision Research.

2.2.3. Exposure to UVB

2.2.3.1. Cell UVB treatment. Cells were washed twice with prewarm phosphate-buffered saline (PBS). After the PBS was removed, the cells were supplied with cold PBS until they were completely covered. The culture dishes were removed, placed on ice and then exposed under a handheld UV lamp (LUYOR LEB-280 L, USA) with a total output of 5 W/m^2 (312 nm) at a fixed distance. The times of exposure were 0, 20, 40, 100, 150, and 200 s to achieve UVB dosages of 0, 100, 200, 500, 750, and 1000 J/m^2, respectively, as measured with a calibrated radiometer. The effective UVB dose range that guaranteed at least 50% cell viability was screened out for subsequent experiments. After UVB exposure, the cells were cultured for 24 h in an incubator at 37 °C with 5% CO_2.

2.2.3.2. Animal UVB treatment. To prove that UVB-induced cataract was related to ferroptosis and MT delayed the progression of cataract induced by UVB. SD rats were randomly divided into a control group (DMSO**:** 20 rats) and three experimental groups (20 rats each for UVB+DMSO, UVB+ferrostatin-1 (Fer-1) and UVB+ MT). Fifteen minutes before exposure, the rats were anaesthetized by intraperitoneal injection of a mixture of 90 mg/kg ketamine and 15 mg/kg xylazine. Then, tropicamide phenylephrine was dropped in both eyes; at the same time, the rats that received drug treatment were injected subconjunctivally (5 μl/eye) with 500 mM Fer-1, 200 mM MT or the same dose of DMSO used to dissolve the drug using a 28-gauge needle and a Hamilton microinjector. After another 5 min, a single eye of every experimental group rat was exposed to UVB (312 nm) 5 W/m^2 for 30 min. Every time, UVB exposure was synchronized with the drug injection, and the frequency was every other day until it was stopped 9 weeks later. The rats were sacrificed by CO_2 asphyxiation, and the eyes were enucleated and placed in prewarmed isosmotic artificial aqueous humor supplemented with 1% penicillin and streptomycin. Then, the lenses were removed with sharpened microdissection scissors under a dissecting microscope. Great care was taken to avoid scratching the lens surface with the scissors. The macroscopic appearance of all the lenses was examined and photographed. Then, the anterior capsule of each lens was extracted by central continuous circular capsulorhexis and tested in subsequent experiments.

2.2.4. Knockdown and overexpression of SIRT6 locally in vivo

To demonstrate that the difference in SIRT6 expression was the underlying cause of the opacity of lens alleviated by MT, we randomly divided SD rats into UVB+MT+Control, UVB+MT+si-SIRT6 (or si-Control), and UVB+DMSO, UVB+OE-SIRT6(or OE-Control), UVB+MT+OE-SIRT6. To knock down and overexpress SIRT6 in vivo, 20 adult rats were transfected with SIRT6 siRNA or SIRT6 overexpression vectors and their respective negative controls via subconjunctival injection every fourth day. One eye of each rat received si-control RNA or control vectors, and the other eye received SIRT6 siRNA or SIRT6 overexpression vectors with Polyplus in vivo-jetPEI® (Polyplus, Illkirch, France) as a transfection reagent. The N/P ratio was 6. All the detailed sequence information is summarized in Tables 1 and 2. In brief, siRNA (25 μg) or plasmid DNA (25 μg) was mixed with 50 μl of transfection solution containing 3 μl in vivo-jetPEI®, and 5 μl of complex was injected subconjunctivally into each eye each time. After injection, the eyes of the rats continued to be treated with or without UVB and MT as mentioned above.

2.2.5. Cell Counting Kit-8 (CCK-8) assay

Cells were seeded in 96-well plates at 1×10^4 cells/well and treated with a UVB dose of 0, 100, 200, 500, 750, or 1000 J/m^2 and DMSO, Fer-1, Z-VAD-FMK, Phenoxodiol, Lobaplatin, M50054, QM31 or MT and maintained for 24 h at 37 °C. Ten microlitres of CCK-8 solution was added to each well, and the cells were incubated at 37 °C for 3 h following the manufacturer's instructions. The optical density (OD) at 450 nm was evaluated using a microplate reader. The data are representative of three individual experiments in triplicate.

2.2.6. Real-time polymerase chain reaction (RT—PCR)

GPX4, ferritin heavy chain (FTH1), SLC7A11 and SIRT6 mRNA expression was determined by RT—PCR using SYBR Green detection reagents. All the primer sequences are shown in Table 4. Total RNA was isolated and reverse-transcribed into cDNA with EasyScript® reverse transcriptase (Transgen Biotech, Beijing, China) under the conditions described in the manual. RT—PCR amplification was performed in a 10 μl reaction volume containing 700 ng of cDNA, 3.6 μl of H_2O, 5 μl of TransStart® Green qPCR SuperMix (Transgen Biotech, Beijing, China), 0.2 pM forward primer and 0.2 pM reverse primer. RT—PCR was performed using a real-time PCR system (Bio-Rad, Hercules, CA, USA). The mRNA expression level was normalized with reference to the amount of a housekeeping gene (GAPDH or Lamin B1) using the $2^{-\Delta\Delta Ct}$ method.

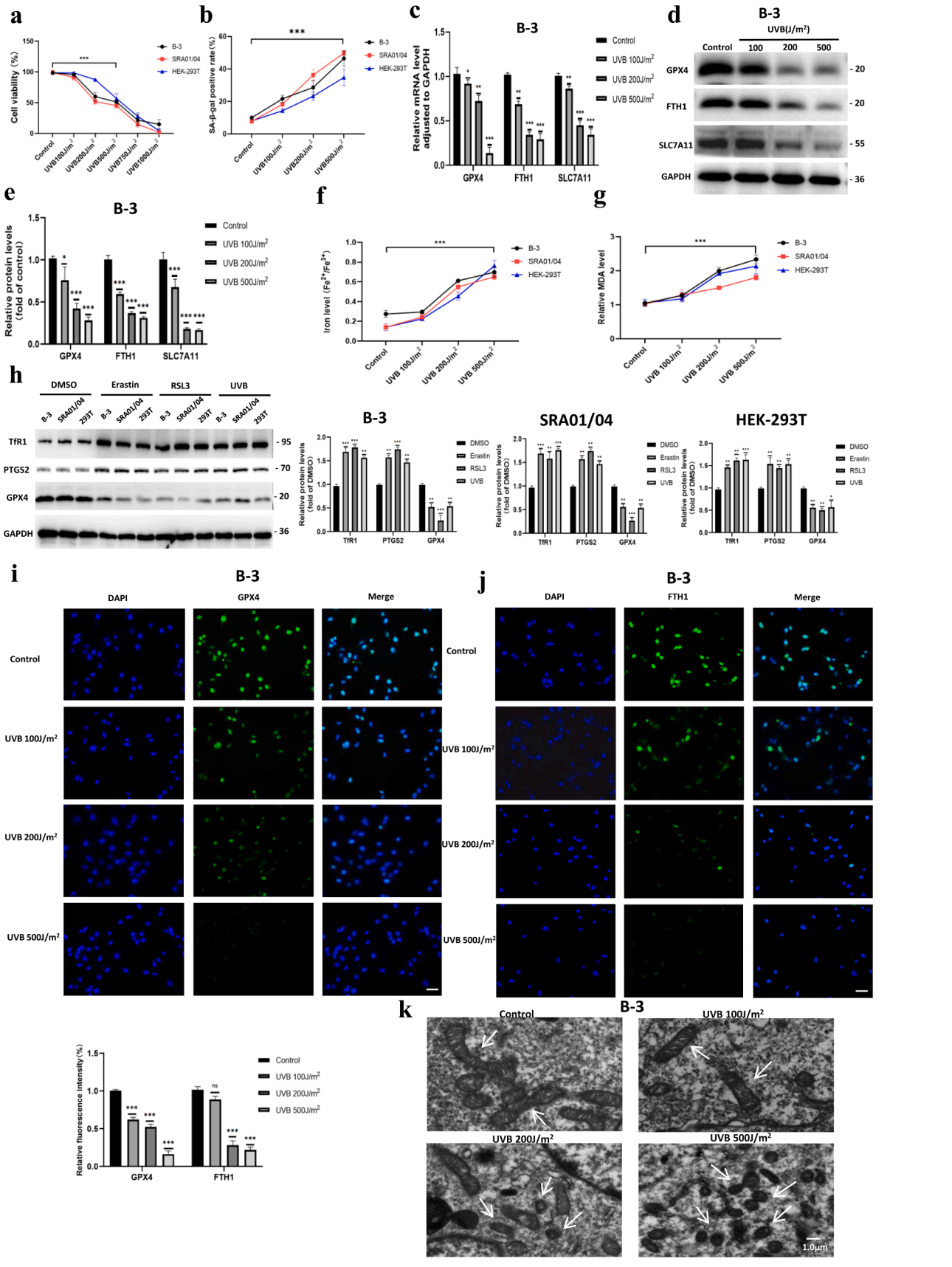

(caption on next page)

Fig. 1. Ferroptosis was induced in B-3, SRA01/04 and HEK-293 T cells dose-dependently by UVB exposure. (a) CCK-8 assay results of B-3, SRA01/04 and HEK-293 T treated cumulatively with increasing amounts of UVB. Three independent experiments. (b) Results of SA-β-gal activity when B-3, SRA01/04 and HEK-293 T cells were exposed to 0, 100, 200 or 500 J/m^2 UVB. (c-e) Results of RT—PCR and western blot analysis for GPX4, FTH1 and SLC7A11 when B-3, SRA01/04 and HEK-293 T cells were exposed to 0, 100, 200 or 500 J/m^2 (compared to control). Three independent experiments. (f-g) Iron level (Fe^{2+}/Fe^{3+}) and relative lipid peroxidation (MDA) level in B-3, SRA01/04 and HEK-293 T cells exposed to increasing UVB doses (compared to control). Three independent experiments. (h) Results of western blot analysis for TfR1, PTGS2 and GPX4 when B-3, SRA01/04 and HEK-293 T cells were treated with DMSO, Erastin, RSL3 and UVB (compared to DMSO). Three independent experiments. (i-j) IF staining and the relative fluorescence intensity of GPX4 and FTH1 in B-3 cells treated with increasing UVB doses (compared to control). Scale bar, 40 μm. Three independent experiments. (k) Results of TEM when B-3 cells were exposed to 0, 100, 200 or 500 J/m^2 UVB. Scale bar, 1 μm; × 8.0k magnification. *P < 0.05, **P < 0.01 and ***P < 0.001.

The data are representative of three individual experiments in triplicate.

2.2.7. Isolation of nuclear, cytoplasmic and cytomembrane extracts

Nuclear extraction was performed using a Nuclear and Cytoplasmic Protein Extraction Kit (Transgen Biotech, Beijing, China) according to the manufacturer's instructions. Briefly, after harvesting the cells and washing the cell pellet twice, 200 μl of ice-cold cytoplasmic extraction buffer (CPEB) I was added, and the mixture was vortexed. The suspension was incubated on ice for 10 min, and 11 μl of CPEB II was added. Then, the mixture was vortexed for 5 s, incubated on ice for 1 min and centrifuged for 8 min at 13,000 × *g*. The supernatant (cytoplasmic extract) was immediately transferred to a prechilled tube. The insoluble (pellet) fraction, which contained the nuclei, was resuspended in 100 μl of nuclear protein extraction buffer by vortexing and then centrifuged for 15 min at 13,000 × *g*. The resulting supernatant, rich in nuclear protein, was used for the following experiments.

Cytomembrane extraction was performed using a Pierce™ Cell Surface Protein Biotinylation and Isolation Kit (Thermo Fisher Scientific, Inc., Waltham, MA, USA). Briefly, add 10 mL of the biotin solution to one 15 cm dish and cells were scraped into solution. Then centrifuge cells at 500 × *g* for 3 min at 4 °C and discard supernatant. Cell pellet was subsequently lysed with 500 μl of Lysis Buffer contained protease inhibitors and then centrifuge cell lysate at 15,000 × *g* for 5 min at 4 °C, transfer clarified supernatant to a new 1.5 mL tube. Then clarified supernatant was used to capture the labeled protein by 250 μl NeutrAvidin agarose. In order to elute proteins, mix 225 μl Elution Buffer and 25 μl Dithiothreitol (DTT) stock solution and add 200 μl to the resin and cap the column. Then incubate the mixture for 30 min at room temperature with end-over-end mixing on a rotator. Then loosen the top cap, remove the bottom cap, place into a collection tube and centrifuge column for 2 min at 1000 × *g*. Add sample buffer to the eluate and analyze by the following experiments.

2.2.8. Western blot analysis

For whole-cell protein extraction, in brief, sample lysates were extracted using radioimmunoprecipitation assay (RIPA) buffer (Boston BioProducts, USA) with 1 mM PMSF. After the cells were vortexed gently, the cell debris was removed by centrifugation at 12,000 × *g* for 15 min

Before electrophoresis, the protein concentrations of the samples were quantified with a Pierce™ BCA Protein Quantification Kit (Thermo Fisher Scientific, Inc., Waltham, MA, USA). For western blotting, protein (50 μg) per sample was separated by 12.5% or 7.5% SDS—PAGE and transferred to a PVDF membrane (Millipore, Darmstadt, Germany). The membranes were blocked with 5% skim milk in Tris-buffered saline containing 0.05% Tween 20 (TBS-T) and incubated with the primary antibodies diluted in TBS-T at 4 °C overnight. The primary antibodies included rabbit anti-GPX4 (Abcam Cat# ab125066, RRID: AB_10973901), rabbit anti-FTH1 (Novus Cat# NBP1–31944, RRID: AB_10003879), rabbit anti-solute carrier family 7 member 11 (SLC7A11) (Novus Cat# NB300–318, RRID: AB_10000581), rabbit anti-SIRT6 (Proteintech Cat# 13572–1-AP, RRID: AB_2188915), rabbit anti-NCOA4 (Affinity Biosciences Cat# DF4255, RRID: AB_2836606), rabbit anti-phospho-Nrf2 S40 (ABclonal Cat# AP1133, RRID: AB_2864001), rabbit anti-Nrf2 (Proteintech Cat# 16396–1-AP, RRID:AB_2782956), rabbit anti-GAPDH (Proteintech Cat# 10494–1-AP, RRID: AB_2263076), rabbit anti-transferrin receptor protein 1 (TfR1) (Proteintech Cat# 10084–2-AP, RRID: AB_2240403), rabbit anti- Na,K-ATPase (Proteintech Cat# 14418–1-AP, RRID: AB_2227873) and rabbit anti-Lamin B1 (Proteintech Cat# 12987–1-AP, RRID: AB_2136290). Subsequently, the membranes were incubated with HRP-conjugated goat anti-rabbit IgG (Thermo Fisher Scientific Cat# 31463, RRID: AB_228333). The antibody–antigen complex was visualized using an Enhanced Chemiluminescent Kit (BL520A Biosharp). GAPDH, Lamin B1 and Na,K-ATPase were used as loading controls. The results are representative of three individual experiments in triplicate.

2.2.9. Immunofluorescence staining

Cells were seeded in 24-well plates at a density of 2.5 × 10^5 cells/well. After treatment for 24 h, the cells were fixed with 4% paraformaldehyde and permeabilized with 0.3% Triton for 15 min. Then, the cells were blocked with 5% normal goat serum (Biosharp, China) and incubated with the following primary antibodies: rabbit anti-GPX4 (Abcam Cat# ab125066, RRID: AB_10973901) (1:150), rabbit anti-FTH1 (Novus Cat# NBP1–31944, RRID: AB_10003879) (1:150), mouse anti-SIRT6 (Abcam Cat# ab119007, RRID: AB_10899478) (1:200), rabbit anti-NCOA4 (Affinity Biosciences Cat# DF4255, RRID: AB_2836606) (1:150), and rabbit anti-Lamin B1 (Proteintech Cat# 12987–1-AP, RRID: AB_2136290) (1:400), rabbit anti-transferrin receptor protein 1 (TfR1) (Proteintech Cat# 10084–2-AP, RRID: AB_2240403) (1:400). The cells were rinsed 3 times in PBS and incubated with H&L (Alexa Fluor® 488) goat anti-rabbit IgG (Abcam Cat# ab150081, RRID: AB_2734747) (1:5000) and H&L (CoraLite® 594) donkey anti-mouse IgG (Proteintech Cat# SA00013–7, RRID: AB_2890973) (1:8000) secondary antibodies for 1 h at room temperature in the dark. Staining was observed using an Observer A1 fluorescence microscope (Zeiss GmbH, Jena, Germany), and ZEN microscope software (ZEN Digital Imaging for Light Microscopy, RRID:SCR_013672) was used. The results are representative of three individual experiments in triplicate.

2.2.10. Immunohistochemical staining

Fresh lens anterior capsules from rats were fixed with 4% paraformaldehyde, permeabilized with 0.3% Triton X-100, and then blocked with 5% BSA. Slides were subsequently incubated with the following primary antibodies: rabbit anti-GPX4 (Abcam Cat# ab125066, RRID: AB_10973901) (1:150), rabbit anti-FTH1 (Novus Cat# NBP1–31944, RRID: AB_10003879) (1:100) and rabbit anti-SIRT6 (Proteintech Cat# 13572–1-AP, RRID: AB_2188915) (1:150). The slides were washed with PBST, and a Universal Mouse/Rabbit Enhanced Polymer Two-Step Detection Kit (ZSGB-BIO, Beijing, China) was applied. Then, staining was performed with 3,3′-diaminobenzidine. The samples were dehydrated in graded ethanol. Staining was observed using an Observer A1 fluorescence microscope (Zeiss GmbH, Jena, Germany), and ZEN microscope software version 2.0 (ZEN Digital Imaging for Light Microscopy, RRID:SCR_013672) was used to take photographs.

2.2.11. Iron assay

The intracellular iron concentration was measured with an Iron Assay Kit (BioVision, SF, USA). Following the manufacturer's instructions, 5 μl of iron reducer was added to the samples to reduce Fe^{3+} to Fe^{2+}, and the samples were incubated for 30 min at room temperature

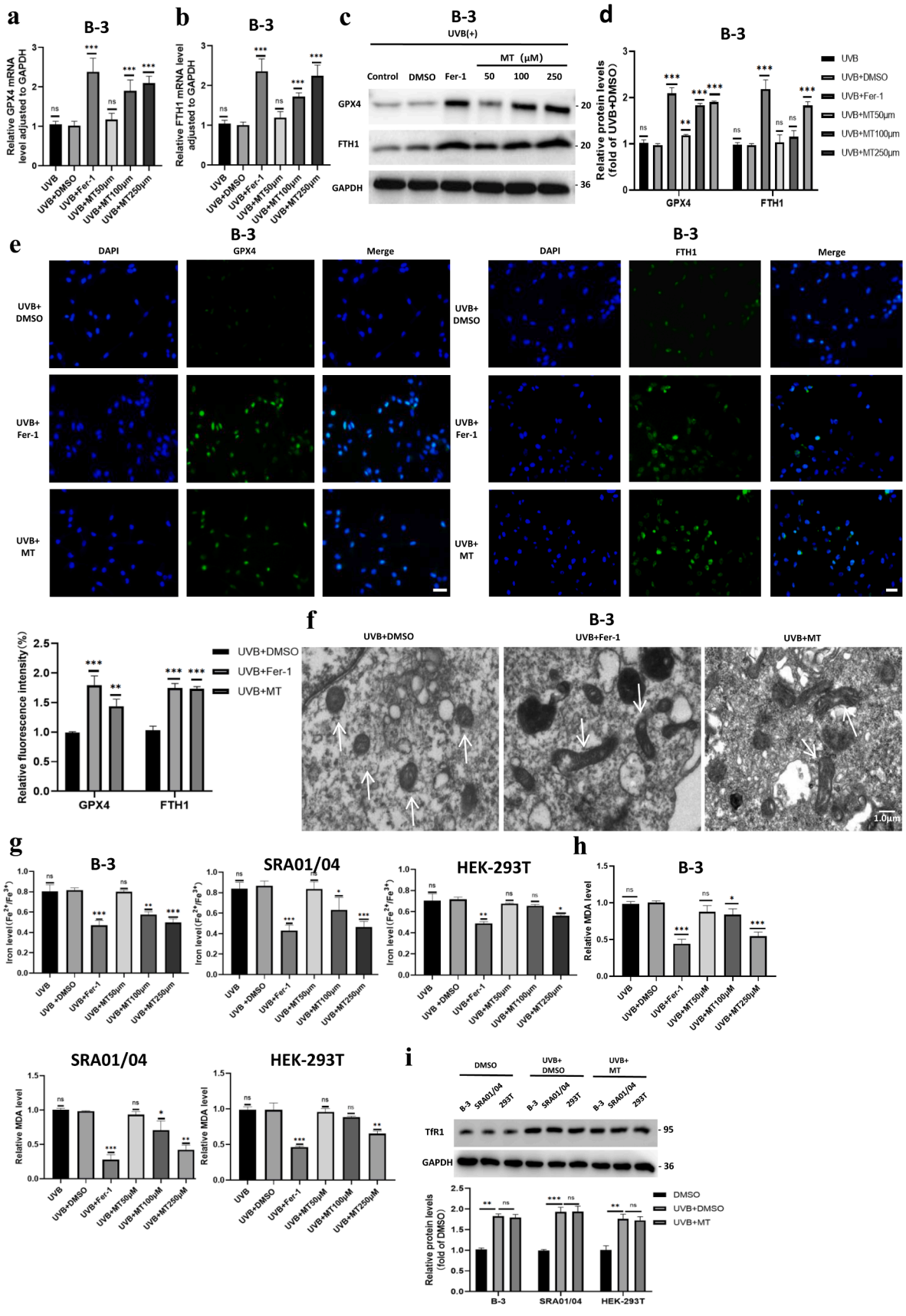

(caption on next page)

Fig. 2. MT inhibited ferroptosis in B-3, SRA01/04 and HEK-293 T cells. (a-d) RT—PCR and western blot analysis results for GPX4 and FTH1 in B-3 cells treated with DMSO, Fer-1, and MT at restricted concentration intervals under UVB exposure (compared to UVB+DMSO). Three independent experiments. (e) IF staining and relative fluorescence intensity of GPX4 and FTH1 in B-3 cells treated with UVB+DMSO, UVB+Fer-1 and UVB+MT (compared to UVB+DMSO). Scale bar, 40 μm. Three independent experiments. (f) Results of TEM when B-3 cells were treated with DMSO, Fer-1 and MT under 500 J/m^2 UVB exposure. Scale bar, 1 μm; × 8.0k magnification. (g-h) Iron level (Fe^{2+}/Fe^{3+}) and relative MDA level in B-3, SRA01/04 and HEK-293 T cells treated with DMSO, Fer-1, and MT at restricted concentration intervals under UVB exposure (compared to UVB+DMSO). Three independent experiments. (i) Results of western blot analysis for total TfR1 when B-3, SRA01/04 and HEK-293 T cells were treated with DMSO, UVB+DMSO and UVB+MT (compared to UVB+DMSO). Three independent experiments. *P < 0.05, **P < 0.01 and ***P < 0.001.

in darkness. The reaction was terminated with an iron probe. The OD value at 593 nm was evaluated using a microplate reader. The data are representative of three individual experiments in triplicate.

2.2.12. Lipid peroxidation assay

The malondialdehyde (MDA) amounts in the supernatants from lysed cells were assessed using an MDA Assay Kit (Beyotime Institute of Biotechnology, Nantong, China) according to the manufacturer's instructions. The fluorescence intensity was measured at 532 nm by an FLx800 fluorescence reader (BioTek, Winooski, VT, USA). The data are representative of three individual experiments in triplicate.

2.2.13. Senescence-associated β-galactosidase (SA-β-gal) activity

SA-β-gal activity was performed by using a commercial assay kit (Cell Signaling, #23833). Cells were seeded in a tissue culture vessel and treated with a UVB dose of 0, 100, 200 or 500 J/m^2. Wash the cells once with cold 1X PBS and add cold 1X senescent cell lysis buffer supplemented with 1.0 mM PMSF and protease inhibitor mixture, and then scrape the cells from the surface and transfer the entire lysate to a microcentrifuge tube. Place the tube into the centrifuge and spin 14,000 × *g* at 4 °C for 5 min, and then transfer 50 μl of supernatant into a 96-well plate. Add 50 μl of 2X detection buffer and incubate the samples at 37 °C protected from light for 2 h. Then pipette 50 μl of the reaction mixture and transfer to a 96-well black opaque plate, stop the reaction by adding 200 μl of Senescence Stop Solution to each well. The fluorescence intensity was measured at an excitation wavelength of 360 nm and an emission wavelength of 465 nm by an FLx800 fluorescence reader (BioTek, Winooski, VT, USA). The data are representative of three individual experiments in triplicate.

2.2.14. Transmission electron microscopy (TEM)

Briefly, treated cells were collected into a centrifuge tube and separated at 3000 × *g* for 8 min. Then, the cells were fixed in 2.5% glutaraldehyde (v/v) in 0.1 M cacodylate buffer (pH 7.2) and osmium tetroxide (1%). The samples were then cut and stained with 2% uranyl acetate (UA), dehydrated in acetone solutions at increasing concentrations, embedded in an epoxy resin and processed for TEM. Ultrastructural images were then captured with a transmission electron microscope (H-7700, Hitachi High-Technologies, Tokyo, Japan) using a 100 kV accelerating voltage by a histologist who was experienced in TEM.

2.2.15. Caspase activation assay

B-3, SRA01/04 and HEK-293 T cells were seeded at 1 × 10^4 cells/well in 96-well plates and treated with vehicle, UVB, Phenoxodiol or Z-VAD-FMK. Caspase 3/7 activation was measured by using the Caspase-Glo® 3/7 Assay Systems (Promega, Madison, WI, USA). Briefly, 100 μl of Capase-Glo 3/7 Reagent was added to cells directly for another 1.5 h at room temperature and the luminescence intensity was recorded at 570 nm by using a GloMax® Discover Microplate Reader. To measure cleaved caspase 3 activation in treated B-3, SRA01/04 and HEK-293 T cells, the Pathscan Cleaved Caspase-3 Sandwich ELISA Kit (Cell Signaling Technology) was used following the manufacturer's protocol. The level of cleaved caspase-3 was determined by reading OD at 450 nm using a microplate reader. The data are representative of three individual experiments in triplicate.

2.2.16. Statistical analysis

The experimental data were first analyzed for normality and lognormality by Shapiro–Wilk test, and then statistical significance was determined by one-way ANOVA. Statistical tests were carried out by GraphPad Prism 8.0 version (GraphPad Prism, RRID: SCR_002798), and $P < 0.05$ was considered to indicate significance. The bars in the graphs represent the means ± SEMs. (*, $p < 0.05$; **, $p < 0.01$; ***, $p < 0.005$; $^{\#}$, $P < 0.05$; $^{\#\#}$, $P < 0.01$ and $^{\#\#\#}$, $P < 0.001$.).

3. Results

3.1. Ferroptosis was induced in B-3, SRA01/04 and HEK-293 T cells via dose-dependent UVB exposure

First, to select the optimal UVB range acceptable to cells, we treated B-3, SRA01/04 and HEK-293 T cells with several different UVB irradiances and detected the cell survival rate by CCK-8 assay. The viability of B-3, SRA01/04 and HEK-293 T cells was inhibited gradually when the cells were treated cumulatively with 0, 100, 200, 500, 750 and 1000 J/m^2 UVB, as indicated by CCK-8 assay (Fig. 1a). Given that 500 J/m^2 was the limit to ensure 50% cell survival, we chose the UVB irradiance range of 0–500 J/m^2 for subsequent experiments. Next, we detected the endogenous SA-β-gal (pH 6.0) activity. SA-β-gal activity was significantly increased via dose-dependent UVB treatment compared with unirradiated cells (Fig. 1b). Molecularly, the expression levels of GPX4, FTH1 and SLC7A11 were decreased in UVB-exposed B-3 cells in a dose-dependent manner (Fig. 1c-e). Compared with that in the negative control group, the relative expression of GPX4, FTH1 and SLC7A11 was decreased by more than 50% when the energy of UVB exposure was 500 J/m^2. Meanwhile, the levels of Iron (Fe^{2+}/Fe^{3+}) and lipid peroxidation in the cytoplasm (Fig. 1f-g) were increased in UVB-exposed B-3, SRA01/04 and HEK-293 T cells in a dose-dependent manner. In addition, compared with DMSO group, UVB, as well as ferroptosis specific agonists Erastin and RSL3, could induce differential protein expression of TfR1, PTGS2 and GPX4, three of the identified ferroptosis markers in B-3, SRA01/04 and HEK-293 T cells (Fig. 1h). Interestingly, consistent with the results of Stockwell, B. R. et al [29]., the expression of whole cell TfR1 and cytomembrane TfR1 were increased in B-3, SRA01/04 and HEK-293 T cells treated with 500 J/m^2 UVB irradiation, while TfR1 in the cytoplasm was decreased, suggesting that part of TfR1 in the cytoplasm was recruited to the cytomembrane during ferroptosis. This was beneficial for the cells to take in more exogenous iron ions (Fig. S2c). Morphologically, with increasing UVB exposure energy, the volume of B-3 cells' mitochondria decreased, the membrane density increased, and the mitochondrial cristae decreased in size, while the change in the nucleus was not obvious (Fig. 1k). Furthermore, the immunofluorescence results (Fig. 1i-j) also suggested that UVB-induced ferroptosis-like symptoms in cells were significantly enhanced in a dose-dependent manner.

3.2. MT inhibited ferroptosis in B-3, SRA01/04 and HEK-293 T cells

To verify whether the cell damage caused by UVB irradiation was due to ferroptosis, cells were treated with Fer-1, a selective ferroptosis inhibitor, and the effect was confirmed. The results showed that the expression levels of GPX4 and FTH1 were significantly rescued by Fer-1 compared with those in the 500 J/m^2 UVB-only group, indicating that

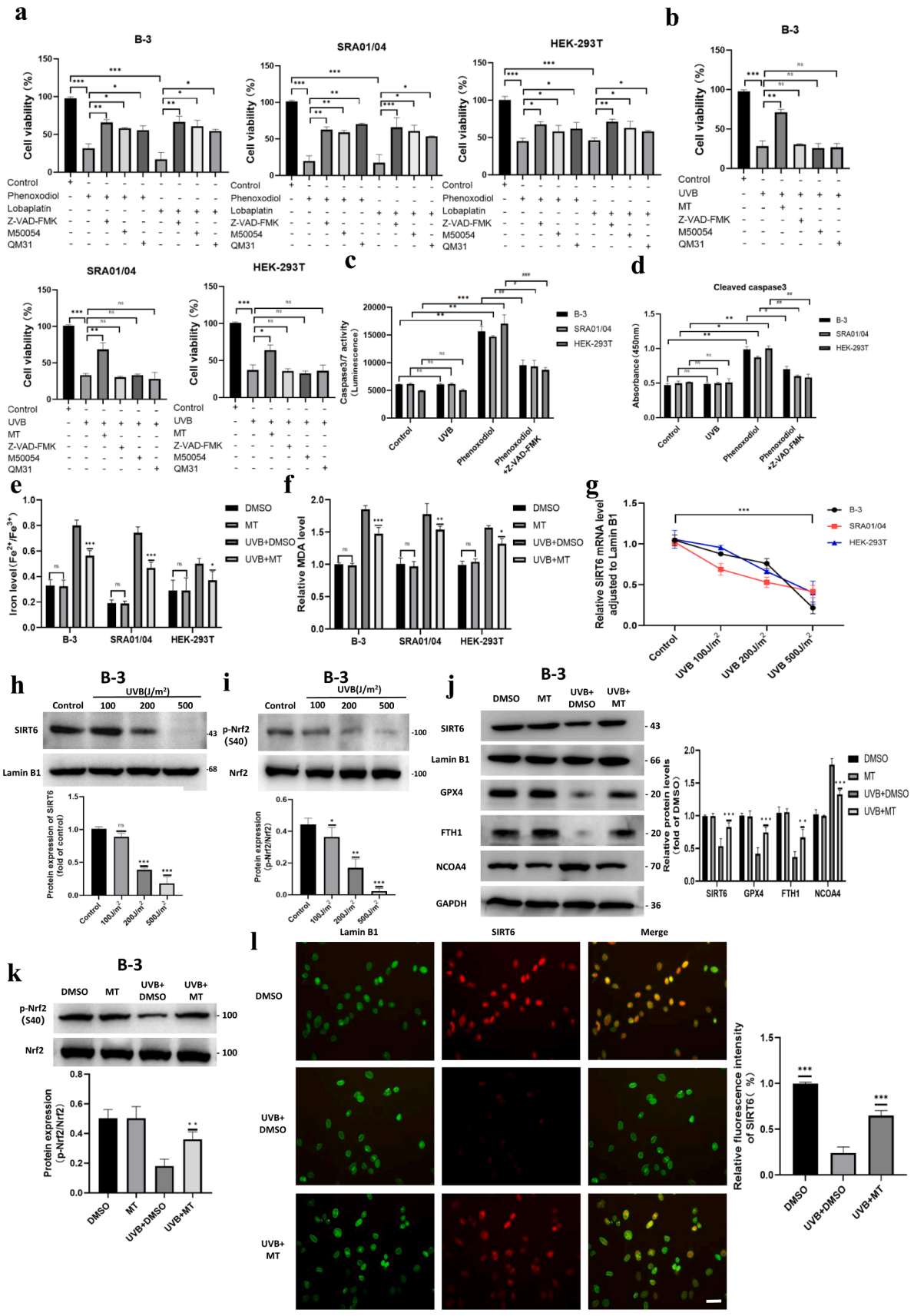

(caption on next page)

Fig. 3. MT alleviated ferroptosis in B-3, SRA01/04 and HEK-293 T cells and was regulated by SIRT6 and p-Nrf2. (a-b) CCK-8 assay results for B-3, SRA01/04 and HEK-293 T cells treated with or without UVB, MT, Phenoxodiol, Lobaolatin, Z-VAD-FMK, M50053 and QM31 (compared to Control, Phenoxodiol, Lobaolatin or UVB). Three independent experiments. (c) Caspase activation (caspase 3/7 and cleaved caspase 3) assay results for B-3, SRA01/04 and HEK-293 T cells treated with UVB, Phenoxodiol, Phenoxodiol+Z-VAD-FMK (compared to Control or Phenoxodiol). Three independent experiments. (e-f) Iron level (Fe^{2+}/Fe^{3+}) and MDA level in B-3, SRA01/04 and HEK-293 T cells treated with DMSO, MT, UVB+DMSO or UVB+MT (compared to UVB+DMSO). Three independent experiments. (g) Relative mRNA levels of SIRT6 in B-3, SRA01/04 and HEK-293 T cells treated with increasing doses of UVB (compared to control). Three independent experiments. (h-i) Western blot analysis of SIRT6 and p-Nrf2/ Nrf2 in B-3 cells treated with increasing UVB doses (compared to control). Three independent experiments. (j-k) Western blot analysis of SIRT6, GPX4, FTH1, NCOA4 and the level of p-Nrf2/ Nrf2 in B-3 cells treated with DMSO, MT, UVB+DMSO and UVB+MT (compared to UVB+DMSO). Three independent experiments. (l) IF staining and relative fluorescence intensity of SIRT6 in B-3 cells treated with DMSO, UVB+DMSO or UVB+MT (compared to UVB+DMSO). Scale bar, 40 μm. Three independent experiments. *P < 0.05, **P < 0.01 and ***P < 0.001. $^{\#}$P < 0.05, $^{\#\#}$P < 0.01 and $^{\#\#\#}$P < 0.001.

the degree of ferroptosis in cells was effectively alleviated (Fig. 2a-e). In addition, we found that the effect of MT was similar to Fer-1 in suppressing ferroptosis in a dose-dependent manner in B-3 cells by significantly increasing the expression levels of GPX4 and FTH1 (Fig. 2a-e) and we also found the same effect of MT in UVB-exposed SRA01/04 and HEK-293 T cells (Fig. S1a-b). According to the TEM results, the shrivelled mitochondria after UVB exposure were restored in B-3 cells treated with Fer-1 or MT compared with UVB+DMSO-exposed cells and regained their normal features (Fig. 2f). Furthermore, unsurprisingly, the levels of Fe^{2+}/Fe^{3+} and lipid peroxidation in UVB-exposed B-3, SRA01/04 and HEK-293 T cells were reduced after Fer-1 or MT intervention (Fig. 2g-h). The mechanism by which MT exerted its antiferroptotic effect might be mainly through upregulating GPX4 and FTH1, because MT did not reduce the cellular uptake of exogenous iron ions by inhibiting TfR1 in B-3, SRA01/04 and HEK-293 T cells (Fig. 2i, Fig. S2a-c).

3.3. MT alleviated ferroptosis in B-3, SRA01/04 and HEK-293 T cells, and the effect was regulated by SIRT6 and p-Nrf2

It is important to understand the specific types of cell death from which MT protects cells. First, we established a positive control model of apoptosis. Both Phenoxodiol and Lobaplatin (known apoptosis inducers) significantly reduced the viability of B-3, SRA01/04 and HEK-293 T cells, and the cell survival rates were saved by Z-VAD-FMK, M50054 and QM31 (known apoptosis inhibitors), as shown by CCK-8 assay (Fig. 3a). Second, the activation and expression of caspase3/7 and cleaved caspase3 were increased in B-3, SRA01/04 and HEK-293 T cells treated with Phenoxodiol, and were inhibited by Z-VAD-FMK (Fig. 3c-d). However, the expression of caspase3/7 and cleaved caspase3 was not affected in B-3, SRA01/04, and HEK-293 T cells during 500 J/m^2 UVB irradiation (Fig. 3c-d), and the decline of cell viability caused by UVB irradiation was not rescued by Z-VAD-FMK, M50054, and QM31 (Fig. 3b). In addition, despite UVB treatment, the levels of Fe^{2+}/Fe^{3+} and lipid peroxidation were reduced when MT was added compared with that in the UVB+DMSO group (Fig. 3e-f), and all the evidence appeared to suggest that, in the 500 J/m^2 UVB irradiation scheme we provided, apoptosis was not observed but ferroptosis in B-3, SRA01/04, and HEK-293 T cells; MT was effective for ferroptosis induced by UVB. Then, we found that the mRNA and protein levels of SIRT6 and the levels of p-Nrf2/Nrf2 in the nucleus were both decreased in UVB-exposed B-3 cells (Fig. 3g-i). MT significantly rescued SIRT6 and promoted the phosphorylation of Nrf2 after UVB irradiation in B-3, SRA01/04, and HEK-293 T cells compared to UVB+DMSO group (Fig. 3j-l, Fig. S1a-b), and the trend was consistent with the effect on GPX4 and FTH1.

3.4. MT protected B-3, SRA01/04 and HEK-293 T cells from ferroptotic stress by activating the SIRT6/p-Nrf2/GPX4 pathway

To gain insight into the mechanisms by which MT relieves ferroptotic stress, we identified the upstream regulatory mechanism of GPX4 and FTH1 by cell transfection. First, we confirmed that MT plays an antiferroptotic role by regulating SIRT6 because when cells were under the ferroptotic pressure induced by UVB, despite MT treatment, loss of SIRT6 still aggravated ferroptosis compared with that in the negative control group, as indicated by the observed dynamic downregulation of the key phenotypic factors GPX4 and FTH1 (Fig. 4a, c). The results of TEM also supported this result in terms of morphology (Fig. 4b). Next, we studied the regulatory relationships among SIRT6, Nrf2, GPX4 and FTH1 in detail. The SIRT6 and Nrf2 genes were silenced and overexpressed by transient transfection of siRNA and an overexpression plasmid vector, respectively, and the expression of several other proteins was observed. Not surprisingly, we found that when SIRT6 was silenced or overexpressed under UVB-driven ferroptotic stress, the level of the p-Nrf2/ Nrf2, GPX4 and FTH1 proteins in B-3, SRA01/04 and HEK-293 T cells remained synchronized (Fig. 4d, Fig. S3a-d). However, when we silenced or overexpressed Nrf2 to indirectly obtain low or high expression levels of p-Nrf2 in the nucleus, the expression of GPX4 was controlled by p-Nrf2(or Nrf2), but that of FTH1 did not change (Fig. 4e). Moreover, when B-3, SRA01/04 and HEK-293 T cells were treated with Erastin to induce ferroptosis and Nrf2 was silenced or overexpressed again, FTH1 expression remained unchanged (Fig. 4f, Fig. S3e-f). This indicates that SIRT6 is the upstream signal of p-Nrf2, GPX4 and FTH1. In addition, p-Nrf2 is an upstream regulatory signal of GPX4 that regulates the expression of GPX4 but not FTH1. There might be another independent signaling pathway by which SIRT6 regulates FTH1.

3.5. MT protected B-3, SRA01/04 and HEK-293 T cells from ferroptotic stress by activating the SIRT6/NCOA4/FTH1 pathway

To explore how SIRT6 regulates FTH1 expression, we prioritized NCOA4, a selective cargo receptor associated with cytoplasmic ferritinophagy that has been identified to interact with ferritin. Similar methods were used to analyze the regulatory relationships among SIRT6, NCOA4 and FTH1. When the SIRT6 gene was silenced or overexpressed under UVB-driven ferroptotic stress, the expression of NCOA4 was also reduced and enhanced in B-3, SRA01/04 and HEK-293 T cells, respectively (Fig. 5a, Fig. S3a-b). However, when the SIRT6 gene was silenced without UVB, the protein expression of NCOA4 was upregulated (Fig. 5b, Fig. S4c-d); when the NCOA4 gene was silenced or overexpressed, SIRT6 expression did not change in B-3, SRA01/04 and HEK-293 T cells as expected (Fig. 5c-d, Fig. S4e-g). In contrast, FTH1 expression was upregulated or downregulated, respectively, due to the classical ferritin autophagy lysosome pathway (Fig. 5c). In addition, although we artificially changed the expression of NCOA4 via genetic engineering, GPX4 and the level of p-Nrf2/Nrf2 remained at their original levels (Fig. 5c). When B-3 cells were induced to undergo ferroptosis with UVB, compared with the negative control group, the NCOA4-overexpressing group still exhibited morphological signs of ferroptosis, even if these two groups were both treated with MT in advance (Fig. 5e); this result indicated that MT could indirectly downregulate the ferritin autophagy pathway by inhibiting the expression of NCOA4. Moreover, when we silenced and overexpressed NCOA4 again and then induced ferroptosis in B-3, SRA01/04 and HEK-293 T cells with Erastin, the expression of GPX4 remained unchanged (Fig. 5f, Fig. S4a-b). Blockade of either of the two SIRT6 pathways (Nrf2 or NCOA4) alone did not interfere the positive effect of MT on the viability of B-3, SRA01/04 and HEK-293 T cells suffered to ferroptotic stress induced by UVB; When the two branched pathways controlled by SIRT6 (Nrf2 and NCOA4) were both blocked, there was no medicinal value with or

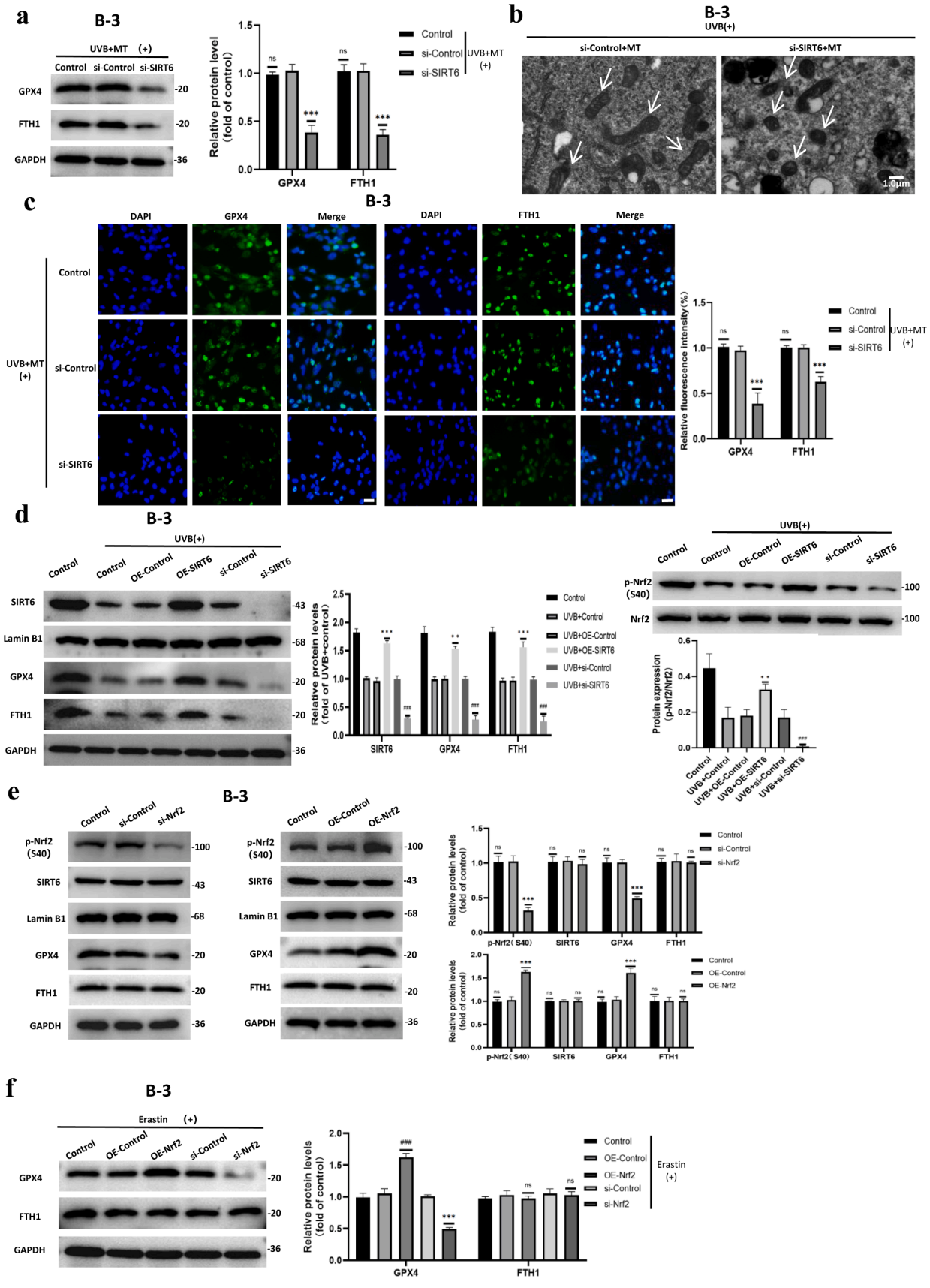

(caption on next page)

Fig. 4. MT protected B-3, SRA01/04 and HEK-293 T cells from ferroptotic stress by activating the SIRT6/p-Nrf2/GPX4 pathway. (a) B-3 cells transfected with either control siRNA or SIRT6 siRNA were then treated with UVB+MT. The results of Western blot analysis and the relative protein levels of GPX4 and FTH1 are shown (compared to si-Control). Three independent experiments. (b) TEM results in B-3 cells transfected with either control siRNA or SIRT6 siRNA and then treated with UVB+MT. Scale bar, 1 μm; × 8.0k magnification. (c) IF staining and relative fluorescence intensity of GPX4 and FTH1 in B-3 cells transfected with either control siRNA or SIRT6 siRNA and then treated with UVB+MT (compared to si-Control). Scale bar, 40 μm. Three independent experiments. (d) B-3 cells transfected with either SIRT6 overexpression (OE) vectors or SIRT6 siRNA and their respective negative controls and then treated with UVB. The results of Western blot analysis and the relative protein levels of SIRT6, GPX4, FTH1 and the level of p-Nrf2/Nrf2 are shown (compared to their negative controls). Three independent experiments. (e) B-3 cells transfected with either OE-Nrf2 vectors or Nrf2 siRNA and their respective negative controls. The results of Western blot analysis and the relative protein levels of SIRT6, GPX4, FTH1 and the level of p-Nrf2/Nrf2 are shown (compared to their negative controls). Three independent experiments. (f) B-3 cells were transfected with either OE-Nrf2 vectors or Nrf2 siRNA and their respective negative controls and then treated with Erastin. The results of Western blot analysis and the relative protein levels of GPX4 and FTH1 are shown (compared to their negative controls). Three independent experiments. $^{*}P < 0.05$, $^{**}P < 0.01$ and $^{***}P < 0.001$. $^{\#}P < 0.05$, $^{\#\#}P < 0.01$ and $^{\#\#\#}P < 0.001$.

without MT (Fig. 5g). These results suggested that MT activated SIRT6/p-Nrf2/GPX4 and SIRT6/NCOA4/FTH1 signaling to play an anti-ferroptotic role by upregulating SIRT6.

3.6. MT relieved ferroptotic stress in lenses and delayed cataract progression in SD rats by activating SIRT6

Based on the above results, we constructed an animal model to verify them in vivo. Regarding macroscopic appearance, the lenses of the DMSO group with no exposure remained transparent throughout the 9-week observation period, which excluded the interference of repeated ocular injections over a long period of time with the lens (Fig. 6-a). However, in the UVB exposure groups, 85% (51/60) of the rats developed cortical cataract of at least the grade of C3N0P1 after 9-week UVB treatment, which was assessed by classical Lens Opacities Classification System III [30] (Fig. 6-a). Interestingly, compared with the UVB-only group, the degree of lens turbidity in rats receiving Fer-1 or MT subconjunctival injection was significantly lower, and only a uniformly distributed polka-dot opacity of the equatorial cortex with a slight haze of epithelial cells was observed (Fig. 6-a). These results suggest that there may be different degrees of ferroptotic stress in the lenses of rats induced by UVB exposure and that MT may suppress ferroptosis as an antioxidant. To further validate these results, the lens anterior capsules of cataract rats exposed to low-dose UVB for up to 9 weeks and negative control samples were collected and analyzed for SIRT6, p-Nrf2/Nrf2, GPX4, FTH1 and NCOA4 expression via immunohistochemical staining, western blot analysis and iron assays. The expression of SIRT6, GPX4, FTH1 and the level of p-Nrf2/Nrf2 was significantly downregulated, but that of NCOA4 was upregulated, in UVB-exposed capsules compared with DMSO-only capsules. However, the levels of these proteins were restored in UVB group rats that received Fer-1 and MT, and this trend was consistent with the immunohistochemical staining of GPX4 and SIRT6 (Fig. 6b-c, e-f). With the results regarding the changes of the levels of Fe^{2+}/Fe^{3+} in capsules, we confirmed the catalytic role of ferroptosis in UVB-induced cataracts in rats (Fig. 6d). Next, to confirm the ferroptotic resistance of SIRT6 in vivo, SIRT6 was artificially knocked out locally in the eyes of rats with a transfection reagent for local injection in vivo. We found via western blot and immunohistochemical analyses that, due to the absence of SIRT6 in the eyes, the expression levels of GPX4 and FTH1 in UVB-exposed cataract capsules treated with MT were significantly lower than those in the negative control transfection capsules (Fig. 6h-i, k-l), which implied that the anti-ferroptosis effect of MT must be mediated by SIRT6. In terms of macroscopic appearance, there were other findings that supported this conclusion that SIRT6-deficient lenses also developed more severe cataracts than SIRT6-sufficient lenses (Fig. 6g). SIRT6 excess significantly alleviated the turbidity of the lenses, and the lenses remained more transparent if MT was used simultaneously (Fig. 6j).

4. Discussion

In this study, we first found that UVB-induced ferroptosis led to ARCs by regulating two SIRT6 signaling pathways. MT inhibited ferroptosis and alleviated ARCs by activating the SIRT6/Nrf2/GPX4 and SIRT6/NCOA4/FTH1 signaling pathways.

UV radiation can cause eye phototoxicity and ageing [31]. Among the UV types, UVB is closely related to oxidative damage to the lens, leading to cataracts [32]. UVB is able to stimulate slow-release oxidative responses that may persist even if the irradiation is stopped. Once these responses happen, the products, such as free radicals ($HO^{\cdot}$, $O_2^{\cdot-}$) that belong to the ROS and the nonradical oxygen species (H_2O_2,$^1O_2$), can trigger a series of oxidative damage reactions in eukaryotic cells [33], including indirect DNA and protein damage, reduction of glutathione, cell membrane pump damage, signal transduction pathway activation and inactivation of the gene expression of some metabolic enzymes [34]. The ageing of the lens is at least largely due to cumulative damage caused by ROS [35], and oxidative stress caused by various sources of stimulation in the lens epithelium is the direct cause of cataracts [36]. However, the specific unit of measurement of UVB irradiance has never been described in detail. In this study, we determined that UVB radiation doses ranging from 0 to 500 J/m^2 could guarantee a survival rate of at least 50%. In addition, we successfully established a 9-week UVB-exposed rat model of cataracts and provided a specific method including the irradiation frequency and dose.

In recent years, increasing numbers of studies have explored the role of ferroptosis, which is a new form of cell death involved in the pathogeneses of various diseases. During this process, blockade of SLC7A11, a subunit of system x_c^-, and its partner subunit solute carrier family 3 member 2 leads to the depletion of intracellular reduced GSH and indirectly impairs glutathione peroxidase 4 (GPX4), a selenoprotein that is an important regulator of ferroptosis and effectively reduces lipid peroxidation. On the other hand, exogenous free Fe^{3+} are taken into the cell by transferrin and TfR1 on the cell surface and acidified to Fe^{2+}. Excessive accumulation of free divalent iron in cells is also one of the key processes of ferroptosis. Fe^{2+} regulates metabolic processes and oxidative stress. The accumulation of free iron ions in cells is also one of the key processes of ferroptosis. Fe^{2+} regulates metabolic processes and oxidative stress. Moreover, Fe^{2+} also binds with intracellular ferritin, including ferritin light chain and FTH1, to form complexes that are stored in cells temporarily. Ferritin is transported to lysosomes by the ferritinophagy-associated selective cargo receptor NCOA4 to maintain intracellular iron homeostasis via self-degradation through the ferritinophagy pathway [37,38]. This causes excessive intracellular Fe^{2+} to promote ferroptosis through the Fenton reaction and produce superfluous ROS to attack the plasma membrane structures of cells [39]. Ferroptosis can be intensified by increasing iron absorption, decreasing iron transport and utilization, or directly damaging ferritin [40]. Free iron accumulation, cysteine metabolism and excessive ROS have become known as important regulators of ferroptosis [41]. However, currently, knowledge of the role of ferroptosis in cataract pathogenesis is scarce. Thus far, there is only evidence that a low dose of the ferroptosis activator erastin and the GPX4 inhibitor RSL3 can induce ferroptosis in the lens epithelium and that the senescence state of cells after 55 generations is highly sensitive to ferroptosis [14]. However, to the best of our knowledge, lens epithelial cells death by ferroptosis under UVB irradiation has never been demonstrated before. This may be due in part

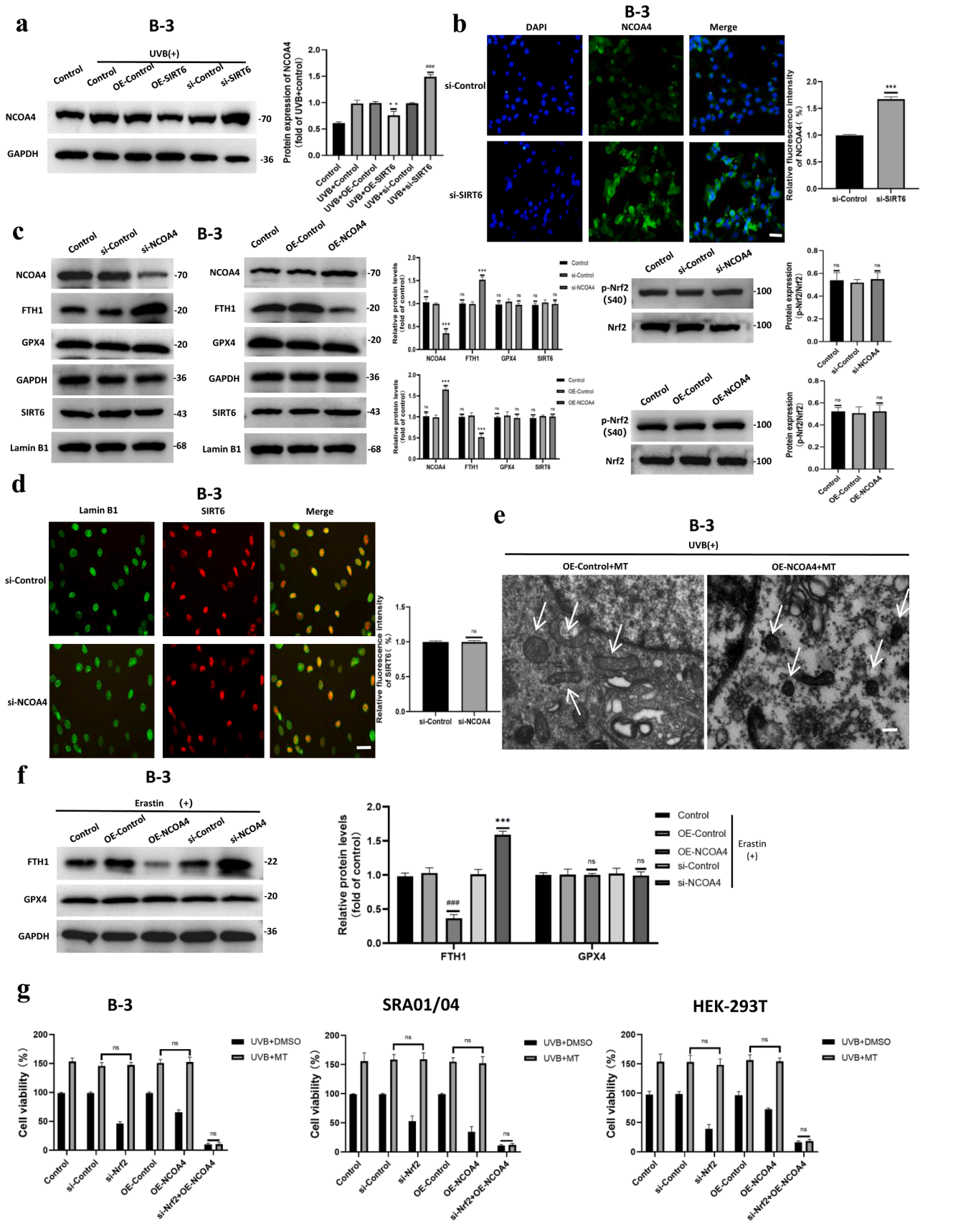

(caption on next page)

Fig. 5. MT protected B-3, SRA01/04 and HEK-293 T cells from ferroptotic stress by activating SIRT6/NCOA4/FTH1 pathway. (a) B-3 cells transfected with either SIRT6 OE vectors or SIRT6 siRNA and their respective negative controls and then treated with UVB. The results of Western blot analysis and the relative protein levels of NCOA4 are shown (compared to their negative controls). Three independent experiments. (b) IF staining and relative fluorescence intensity of NCOA4 in B-3 cells transfected with either control siRNA or SIRT6 siRNA. Scale bar, 40 μm. Three independent experiments. (c) B-3 cells transfected with either NCOA4 OE vectors or NCOA4 siRNA and their respective negative controls, the results of Western blot analysis and the relative protein levels of SIRT6, NCOA4, GPX4, FTH1 and the level of p-Nrf2/Nrf2 are shown (compared to their negative controls). Three independent experiments. (d) IF staining and relative fluorescence intensity of SIRT6 in B-3 cells transfected with either control siRNA or NCOA4 siRNA. Scale bar, 40 μm. Three independent experiments. (e) Results of TEM in B-3 cells transfected with either NCOA4 OE vectors or negative control, and then treated with UVB+MT. Scale bar, 1 μm; × 8.0k magnification. (f) B-3 cells transfected with either NCOA4 OE vectors or NCOA4 siRNA and their negative controls and then treated with Erastin, the results of western blot analysis and relative protein levels of GPX4 and FTH1 were shown (compared to their negative controls). Three independent experiments. (g) B-3, SRA01/04 and HEK-293 T cells with or without MT pretreatment were transfected with either NCOA4 OE vectors or Nrf2 siRNA and their respective negative controls and then treated with UVB. The results of CCK-8 assay are shown (compared to UVB+MT or their negative controls). Three independent experiments. $^{*}P < 0.05$, $^{**}P < 0.01$ and $^{***}P < 0.001$. $^{\#}P < 0.05$, $^{\#\#}P < 0.01$ and $^{\#\#\#}P < 0.001$.

to the difficulty of distinguishing ferroptosis from other modes of regulatory cell death (RCD). Unlike other RCD pathways, the cytotoxicity of ferroptosis is dependent on excessive and specific phosphorylated lipid peroxidation, which is removed by lipid alkoxyl radical scavengers such as Fer-1. Excessive and specific phosphorylated lipid peroxidation attacks and causes mitochondrial disorders directly, changes and deficiency of cellular energy, and then initiates and accelerates ageing. In the case of ageing, the normal ability of cells to overcome oxidative stress decreases, eventually leading to a cellular degradation process. In a similar manner, the normal antioxidant defense mechanisms of lens epithelial cells are unable to overcome the oxidative stress induced by ferroptosis and this process is crucial in the pathogenesis of ARCs. Recently, researchers demonstrated in nematode models that ferroptosis was a pervasive and key feature that promoted and accelerated the ageing process [42]. Therefore, it is rationalized to speculate that ferroptosis is expected to participate in the ageing of lens epithelium and ARCs process. Another pendent question is whether UVB has the ability to induce ferroptosis in lens epithelial cells, although our eyes are inevitably exposed to UV radiation in daily life. In this study, we searched for and finally identified the optimal dose range for UVB radiation to cause oxidative injury in the lens epithelium in vitro and in vivo. Our study has provided a UVB irradiation scheme capable of inducing ferroptosis in cells. We found that ferroptosis was strongly induced by 500 J/m^2 UVB irradiation in the lens epithelium in a dose-dependent manner, while apoptosis dependent on the regulation of the caspase family was not observed distinctly. However, we do not reject the potential of UVB to induce apoptosis, and future studies should focus on classifying and optimizing UVB irradiation dose and frequency, as well as detecting more time nodes of induction conditions among apoptosis, ferroptosis and other RCDs. In addition, an interesting observation in this study was that, part of TfR1 protein in the cytoplasm was recruited back to the cell surface during UVB-induced ferroptosis and it was consistent with study of Stockwell, B. R [29]. A plausible explanation for this was that the process might make preparations for taking in more exogenous iron ions through a positive feedback cycle between iron uptake and ferroptotic death.

SIRT6, an NAD^+-dependent enzyme, is a member of the sirtuin family that can protect against ageing-associated pathologies and promote longevity in mice [43]. A recent study found that the expression of SIRT6, at both the mRNA and protein levels, is significantly increased after treatment with melatonin and that SIRT6 protects against cardiac remodeling after myocardial injury [44]. Silencing of SIRT6 can promote ferroptosis in gastric cancer [45]. Activation of SIRT6 inhibits inflammation and ferroptosis and reduces depressive-like and anxiety-like behaviors in mice [46]. The natural self-protection mechanisms activated by SIRT6 in cells at the molecular level are overwhelming before the redox balance is disrupted [47]. Under normal physiological conditions, SIRT6 in the nucleus acts as an epigenetic mediator to continuously stimulate downstream antioxidant elements to maintain redox equilibrium [19]. However, we found that the normal function of SIRT6 was disrupted by UVB-induced ferroptotic pressure in human and rat lens epithelia, and eventually, cells underwent ferroptosis, leading to cataract formation. In addition, phosphorylated Nrf2, a known downstream factor of SIRT6, was inhibited by UVB exposure. Fortunately, artificially overexpressing the SIRT6 gene in rat lens tissue via local site-directed transfection was sufficient to delay the progression of UVB-induced cataracts, even though the transparency of the lens was also decreased. Therefore, we concluded that UVB-induced severe ferroptotic damage and redox homeostasis could not be restored by the cells themselves unless an agonist was found that targeted SIRT6.

In vertebrates, MT is centrally synthesized by the pineal gland, a neuroendocrine organ, in addition to being produced by peripheral tissues and acting as an autocrine and paracrine signal [48,49]. In addition to roles in circadian regulation, MT has antioxidant, antiaging, immunomodulatory, and anticancer properties [50]. Intraperitoneal injection of MT inhibits pyroptosis and alleviates depression-like behavior in mice by regulating the expression of the inflammasome complex NLRP3 [51]. The effects of MT on autophagy and apoptosis can prevent oxidative damage in human retinal pigment epithelial cells [52]. Our previous studies have revealed that MT is more effective than the traditional antioxidant vitamin E in inhibiting intracellular ROS production through the PI3K/Akt antiapoptotic signaling pathway in human lens epithelial cells [27]. In this study, we tested for the first time whether MT plays a role when B-3 cells are under ferroptotic stress. Remarkably, the ferroptotic effect elicited by UVB exposure was reversible, as evidenced by the delay in cataract progression following MT supplementation. In detail, we have discovered that MT has a similar effect compared to fer-1 in suppressing ferroptosis not only in B-3 cells but also in lens anterior capsules from cataract rats by upregulating the expression of GPX4 and FTH1. These findings might provide a new way to delay the progression of cataracts or even to treat them nonsurgically. However, it is necessary to explore the specific mechanism of MT-mediated resistance to ferroptosis, that is, how MT significantly upregulates the expression of GPX4 and FTH1. We utilized recent findings that SIRT6 can partly regulate Nrf2 to play an indirect antioxidant role [53–55]. We confirmed the regulatory relationship among SIRT6, p-Nrf2, GPX4 and FTH1 in HLE B-3 cells by cell transfection and western blot analysis. We were able to exploit the finding that MT targets SIRT6 to regulate two downstream signaling pathways in ferroptosis resistance. However, we hypothesized that SIRT6 could regulate downstream GPX4 and FTH1 simultaneously to prevent ferroptosis by activating Nrf2 transport into the nucleus. Interestingly, FTH1 was not controlled by Nrf2. In fact, FTH1 and NCOA4, cargo receptors that mediate selective ferritinophagy, are interacting microcirculatory regulatory proteins. In glioblastoma, high expression of NCOA4 leads to degradation of FTH1, a subsequent increase in intracellular ferrous iron and ultimately ferroptosis [56]. Overexpression of FTH1 in PC-12 cells impairs and downregulates NCOA4 and suppresses cell death induced by ferroptosis [57]. SIRT6 indirectly enhanced the expression of FTH1 by inhibiting NCOA4. Ultimately, we uncovered the molecular mechanism by which MT promotes ferroptosis resistance. Cells that cannot induce SIRT6 and inhibit the process of ferritinophagy are therefore highly sensitive to the induction of ferroptosis. Although this finding demonstrates that MT might play a role in regulating ferritinophagy by

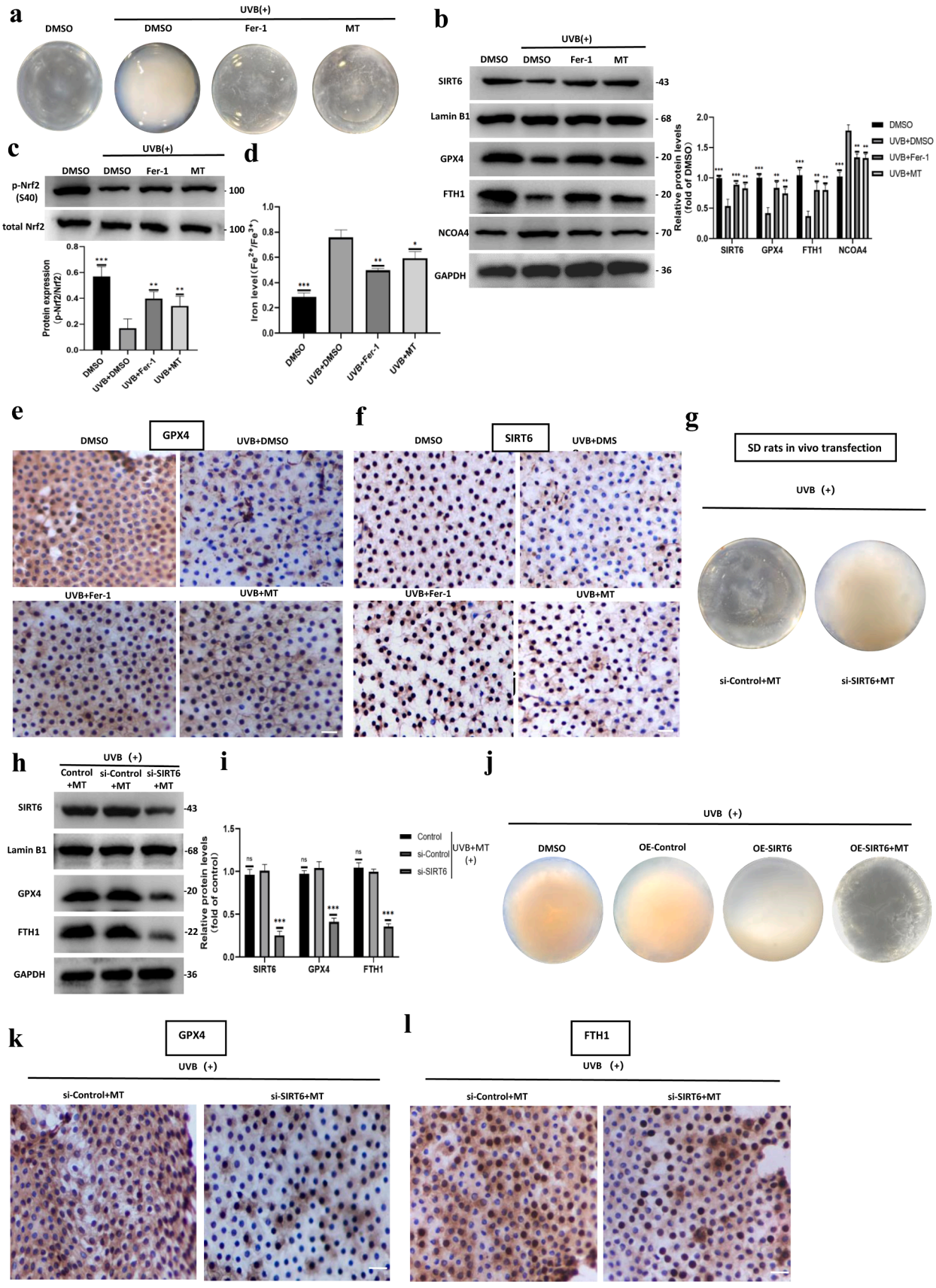

(caption on next page)

Fig. 6. MT relieved ferroptotic stress in lens and delayed cataract progression in SD rats by activating SIRT6. (a) Lenses from SD rats under the light microscope which treated with single eye subconjunctival injection respectively of DMSO, UVB+DMSO, UVB+Fer-1 and UVB+MT for 9 weeks. (b-c) The results of western blot analysis and relative protein levels of SIRT6, NCOA4, GPX4, FTH1 and the level of p-Nrf2/Nrf2 in rats lens capsules (compared to UVB+DMSO). Three independent experiments. (d) Iron level (Fe^{2+}/Fe^{3+}) in lens anterior capsules of SD rats. Three independent experiments. (e-f) Immunohistochemistry (IHC) staining of GPX4 and SIRT6 in rats lens capsules. Scale bar, 100 μm. (g) Lenses from SD rats treated with injection respectively of MT+SIRT6 siRNA or control siRNA under UVB exposure. (h-i) The results of western blot analysis and relative protein levels of SIRT6, GPX4 and FTH1 in lens capsules treated with UVB+MT and in vivo transfection with either control siRNA or SIRT6 siRNA (compared to si-Control). Three independent experiments. (j) Lenses from SD rats treated with injection respectively of DMSO, OE-Control, OE-SIRT6 and MT+OE-SIRT6 under UVB exposure. (k-l) IHC staining of GPX4 and FTH1 in lens capsules treated with injection respectively of MT+SIRT6 siRNA or control siRNA under UVB exposure. *P < 0.05, **P < 0.01 and ***P < 0.001.

upregulating SIRT6, the subsequent events of classical autophagy cannot be ignored, which we will investigate in future studies.

In addition to its direct antioxidant activity, the pharmacological action of MT depends on the signaling regulation mediated by melatonin receptors (belonging to the G-protein coupled receptor family). An increasing number of evidences have shown that melatonin has beneficial effects in age-related degenerative diseases, and it appears that melatonin acts, at least in part, through its receptors MT_1 and MT_2 [58, 59]. They share 60% sequence identity but differ in intracellular signaling pathways. Whether the selective recognition of SIRT6 by MT is regulated by different intracellular signaling pathways mediated by MT1 and MT2 needs to be further verified. In addition, melatonin can prevent receptors loss by itself in some pathological conditions. The mechanism of how melatonin senses and repairs its receptors is a pending issue. Apart from that, it will be interesting to elucidate how UVB, as a kind of radiation, establishes a regulatory link to SIRT6 and exerts a series of molecular biological effects. One possibility is that UVB regulates SIRT6 epigenetically, a process that appears to be critical given that the difference in the gene expression level of SIRT6 was not caused by a change in the gene sequence [60].

In conclusion, our study found that UVB-induced ferroptosis leads to ARCs by downregulating SIRT6 expression. MT alleviates and delays the progression of cataracts by activating the SIRT6/p-Nrf2/GPX4 and SIRT6/NCOA4/FTH1 signaling pathways, respectively. Our study suggests that subconjunctival injection of MT can be used as a more direct and potent nonsurgical therapeutic modality for cataracts than the currently available techniques and that SIRT6 might be a new target for exploring the pathogenesis of cataracts.

Funding

Horizontal Scientific Research Project of Harbin Medical University (Grants: 2020HX033); Innovation and Research Fund of the First Affiliated Hospital of Harbin Medical University (Grants: 2020L02, 2021B14, 2020-KYYWF-1442).

CRediT authorship contribution statement

Hongyan Ge, Ping Liu and Yu Mi designed this study. **Yu Mi, Chaoqun Wei, Liyao Sun and Huirui Liu** performed the in vitro experiments. **Yu Mi, Jialin Luo, Xiaohan Yu and Jie He** performed the in vivo experiments. **Hongyan Ge** guided and supervised this study. **Yu Mi** wrote the manuscript. **Hongyan Ge and Ping Liu** revised the manuscript. All authors read and approved the final version of the manuscript.

Conflict of interest statement

The authors declare that they have no conflict of interest.

Data availability

Data will be made available on request.

Acknowledgments

This work was supported by the Horizontal Scientific Research Project of Harbin Medical University (2020HX033); Innovation and Research Fund of the First Affiliated Hospital of Harbin Medical University (2020L02, 2021B14, 2020-KYYWF-1442).

Data sharing statement

The data generated in this study are made available from the corresponding author upon reasonable request.

Appendix A. Supporting information

Supplementary data associated with this article can be found in the online version at doi:10.1016/j.biopha.2022.114048.

References

[1] Y.C. Liu, M. Wilkins, T. Kim, B. Malyugin, J.S. Mehta, Cataracts, Lancet 390 (10094) (2017) 600–612.
[2] E. Chan, O.A. Mahroo, D.J. Spalton, Complications of cataract surgery, Clin. Exp. Optom. 93 (6) (2010) 379–389.
[3] R. Thiagarajan, R. Manikandan, Antioxidants and cataract, Free Radic. Res. 47 (5) (2013) 337–345.
[4] H.R. Taylor, The biological effects of UV-B on the eye, Photochem. Photobiol. 50 (4) (1989) 489–492.
[5] J. Dairou, F. Malecaze, J.M. Dupret, F. Rodrigues-Lima, The xenobiotic-metabolizing enzymes arylamine N-acetyltransferases in human lens epithelial cells: inactivation by cellular oxidants and UVB-induced oxidative stress, Mol. Pharmacol. 67 (4) (2005) 1299–1306.
[6] Y. Ji, L. Cai, T. Zheng, H. Ye, X. Rong, J. Rao, et al., The mechanism of UVB irradiation induced-apoptosis in cataract, Mol. Cell. Biochem. 401 (1–2) (2015) 87–95.
[7] G.N. Kim, Y.S. Hah, H. Seong, W.S. Yoo, M.Y. Choi, H.Y. Cho, et al., The role of nuclear factor of activated T cells 5 in hyperosmotic stress-exposed human lens epithelial cells, Int. J. Mol. Sci. 22 (12) (2021).
[8] X. Jin, H. Jin, Y. Shi, Y. Guo, H. Zhang, Pyroptosis, a novel mechanism implicated in cataracts, Mol. Med. Rep. 18 (2) (2018) 2277–2285.
[9] T. Hirschhorn, B.R. Stockwell, The development of the concept of ferroptosis, Free Radic. Biol. Med. 133 (2019) 130–143.
[10] B.R. Stockwell, X. Jiang, W. Gu, Emerging mechanisms and disease relevance of ferroptosis, Trends Cell Biol. 30 (6) (2020) 478–490.
[11] B. Lu, X.B. Chen, M.D. Ying, Q.J. He, J. Cao, B. Yang, The role of ferroptosis in cancer development and treatment response, Front. Pharmacol. 8 (2017) 992.
[12] A. Romano, G. Serviddio, S. Calcagnini, R. Villani, A.M. Giudetti, T. Cassano, et al., Linking lipid peroxidation and neuropsychiatric disorders: focus on 4-hydroxy-2-nonenal, Free Radic. Biol. Med. 111 (2017) 281–293.
[13] Y. Yu, L. Jiang, H. Wang, Z. Shen, Q. Cheng, P. Zhang, et al., Hepatic transferrin plays a role in systemic iron homeostasis and liver ferroptosis, Blood 136 (6) (2020) 726–739.
[14] Z. Wei, C. Hao, J. Huangfu, R. Srinivasagan, X. Zhang, X. Fan, Aging lens epithelium is susceptible to ferroptosis, Free Radic. Biol. Med. 167 (2021) 94–108.
[15] L. Tasselli, W. Zheng, K.F. Chua, SIRT6: novel mechanisms and links to aging and disease, Trends Endocrinol. Metab. TEM 28 (3) (2017) 168–185.
[16] J. Kuang, L. Chen, Q. Tang, J. Zhang, Y. Li, J. He, The role of Sirt6 in obesity and diabetes, Front. Physiol. 9 (2018) 135.
[17] Y. Zhou, X. Fan, T. Jiao, W. Li, P. Chen, Y. Jiang, et al., SIRT6 as a key event linking P53 and NRF2 counteracts APAP-induced hepatotoxicity through inhibiting oxidative stress and promoting hepatocyte proliferation, Acta Pharm. Sin. B 11 (1) (2021) 89–99.
[18] L. Li, B. Chen, R. Zhu, R. Li, Y. Tian, C. Liu, et al., Fructus Ligustri Lucidi preserves bone quality through the regulation of gut microbiota diversity, oxidative stress, TMAO and Sirt6 levels in aging mice, Aging 11 (21) (2019) 9348–9368.
[19] H.G. Kim, M. Huang, Y. Xin, Y. Zhang, X. Zhang, G. Wang, et al., The epigenetic regulator SIRT6 protects the liver from alcohol-induced tissue injury by reducing oxidative stress in mice, J. Hepatol. 71 (5) (2019) 960–969.
[20] Z. Jin, Y. Xiao, F. Yao, B. Wang, Z. Zheng, H. Gao, et al., SIRT6 inhibits cholesterol crystal-induced vascular endothelial dysfunction via Nrf2 activation, Exp. Cell Res. 387 (1) (2020), 111744.

[21] S. Rezazadeh, D. Yang, G. Tombline, M. Simon, S.P. Regan, A. Seluanov, et al., SIRT6 promotes transcription of a subset of NRF2 targets by mono-ADP-ribosylating BAF170, Nucleic Acids Res. 47 (15) (2019) 7914–7928.
[22] H. Pan, D. Guan, X. Liu, J. Li, L. Wang, J. Wu, et al., SIRT6 safeguards human mesenchymal stem cells from oxidative stress by coactivating NRF2, Cell Res. 26 (2) (2016) 190–205.
[23] G.L. Sun, D. Huang, K.R. Li, Q. Jiang, microRNA-4532 inhibition protects human lens epithelial cells from ultra-violet-induced oxidative injury via activating SIRT6-Nrf2 signaling, Biochem. Biophys. Res. Commun. 514 (3) (2019) 777–784.
[24] G.A. Bubenik, Gastrointestinal melatonin: localization, function, and clinical relevance, Dig. Dis. Sci. 47 (10) (2002) 2336–2348.
[25] G. Huether, The contribution of extrapineal sites of melatonin synthesis to circulating melatonin levels in higher vertebrates, Experientia 49 (8) (1993) 665–670.
[26] S.U. Rehman, M. Ikram, N. Ullah, S.I. Alam, H.Y. Park, H. Badshah, et al., Neurological enhancement effects of melatonin against brain injury-induced oxidative stress, neuroinflammation, and neurodegeneration via AMPK/CREB signaling, Cells 8 (7) (2019).
[27] J. Bai, L. Dong, Z. Song, H. Ge, X. Cai, G. Wang, et al., The role of melatonin as an antioxidant in human lens epithelial cells, Free Radic. Res. 47 (8) (2013) 635–642.
[28] R. Skouta, S.J. Dixon, J. Wang, D.E. Dunn, M. Orman, K. Shimada, et al., Ferrostatins inhibit oxidative lipid damage and cell death in diverse disease models, J. Am. Chem. Soc. 136 (12) (2014) 4551–4556.
[29] H. Feng, K. Schorpp, J. Jin, C.E. Yozwiak, B.G. Hoffstrom, A.M. Decker, et al., Transferrin receptor is a specific ferroptosis marker, Cell Rep. 30 (10) (2020) 3411–3423, e7.
[30] D.S. Grewal, G.S. Brar, S.P. Grewal, Correlation of nuclear cataract lens density using Scheimpflug images with Lens Opacities Classification System III and visual function, Ophthalmology 116 (8) (2009) 1436–1443.
[31] M. Coroneo, Ultraviolet radiation and the anterior eye, Eye Contact Lens 37 (4) (2011) 214–224.
[32] S. Löfgren, Solar ultraviolet radiation cataract, Exp. Eye Res. 156 (2017) 112–116.
[33] X. Rong, J. Rao, D. Li, Q. Jing, Y. Lu, Y. Ji, TRIM69 inhibits cataractogenesis by negatively regulating p53, Redox Biol. 22 (2019), 101157.
[34] W.C. Li, A. Spector, Lens epithelial cell apoptosis is an early event in the development of UVB-induced cataract, Free Radic. Biol. Med. 20 (3) (1996) 301–311.
[35] R. Michael, A.J. Bron, The ageing lens and cataract: a model of normal and pathological ageing, Philos. Trans. R. Soc. Lond. Ser. B Biol. Sci. 366 (1568) (2011) 1278–1292.
[36] I.V. Ivanov, T. Mappes, P. Schaupp, C. Lappe, S. Wahl, Ultraviolet radiation oxidative stress affects eye health, J. Biophotonics 11 (7) (2018) e201700377.
[37] J.D. Mancias, X. Wang, S.P. Gygi, J.W. Harper, A.C. Kimmelman, Quantitative proteomics identifies NCOA4 as the cargo receptor mediating ferritinophagy, Nature 509 (7498) (2014) 105–109.
[38] M. Goodall, A. Thorburn, Identifying specific receptors for cargo-mediated autophagy, Cell Res. 24 (7) (2014) 783–784.
[39] S. Doll, M. Conrad, Iron and ferroptosis: a still ill-defined liaison, IUBMB Life 69 (6) (2017) 423–434.
[40] G.O. Latunde-Dada, Ferroptosis: role of lipid peroxidation, iron and ferritinophagy, Biochim. Biophys. Acta Gen. Subj. 1861 (8) (2017) 1893–1900.
[41] M.A. Badgley, D.M. Kremer, H.C. Maurer, K.E. DelGiorno, H.J. Lee, V. Purohit, et al., Cysteine depletion induces pancreatic tumor ferroptosis in mice, Science 368 (6486) (2020) 85–89.
[42] N.L. Jenkins, S.A. James, A. Salim, F. Sumardy, T.P. Speed, M. Conrad, et al., Changes in ferrous iron and glutathione promote ferroptosis and frailty in aging Caenorhabditis elegans, eLife (2020) 9.
[43] A. Roichman, S. Elhanati, M.A. Aon, I. Abramovich, A. Di Francesco, Y. Shahar, et al., Restoration of energy homeostasis by SIRT6 extends healthy lifespan, Nat. Commun. 12 (1) (2021) 3208.
[44] Y. Wang, S. Zhang, Y. Ma, A. Xiang, H. Sun, J. Song, et al., Melatonin protected against myocardial infarction injury in rats through a Sirt6-dependent antioxidant pathway, Adv. Clin. Exp. Med. Off. Organ Wroclaw Med. Univ. 31 (3) (2022) 277–284.
[45] S. Cai, S. Fu, W. Zhang, X. Yuan, Y. Cheng, J. Fang, SIRT6 silencing overcomes resistance to sorafenib by promoting ferroptosis in gastric cancer, Biochem. Biophys. Res. Commun. 577 (2021) 158–164.
[46] Y. Wang, S. Wang, Y. Xin, J. Zhang, S. Wang, Z. Yang, et al., Hydrogen sulfide alleviates the anxiety-like and depressive-like behaviors of type 1 diabetic mice via inhibiting inflammation and ferroptosis, Life Sci. 278 (2021), 119551.
[47] C.K. Singh, G. Chhabra, M.A. Ndiaye, L.M. Garcia-Peterson, N.J. Mack, N. Ahmad, The role of sirtuins in antioxidant and redox signaling, Antioxid. Redox Signal. 28 (8) (2018) 643–661.
[48] S. Bhattacharya, K.K. Patel, D. Dehari, A.K. Agrawal, S. Singh, Melatonin and its ubiquitous anticancer effects, Mol. Cell. Biochem. 462 (1–2) (2019) 133–155.
[49] J. Cipolla-Neto, F.G.D. Amaral, Melatonin as a hormone: new physiological and clinical insights, Endocr. Rev. 39 (6) (2018) 990–1028.
[50] F.G.D. Amaral, J. Cipolla-Neto, A brief review about melatonin, a pineal hormone, Arch. Endocrinol. Metab. 62 (4) (2018) 472–479.
[51] B.I. Arioz, B. Tastan, E. Tarakcioglu, K.U. Tufekci, M. Olcum, N. Ersoy, et al., Melatonin attenuates LPS-induced acute depressive-like behaviors and microglial NLRP3 inflammasome activation through the SIRT1/Nrf2 pathway, Front. Immunol. 10 (2019) 1511.
[52] C.C. Chang, T.Y. Huang, H.Y. Chen, T.C. Huang, L.C. Lin, Y.J. Chang, et al., Protective effect of melatonin against oxidative stress-induced apoptosis and enhanced autophagy in human retinal pigment epithelium cells, Oxid. Med. Cell. Longev. 2018 (2018), 9015765.
[53] Y. He, G. Yang, L. Sun, H. Gao, F. Yao, Z. Jin, et al., SIRT6 inhibits inflammatory response through regulation of NRF2 in vascular endothelial cells, Int. Immunopharmacol. 99 (2021), 107926.
[54] F. Gao, M. Qian, G. Liu, W. Ao, D. Dai, C. Yin, USP10 alleviates sepsis-induced acute kidney injury by regulating Sirt6-mediated Nrf2/ARE signaling pathway, J. Inflamm. 18 (1) (2021) 25.
[55] Y. Fan, J. Cheng, Q. Yang, J. Feng, J. Hu, Z. Ren, et al., Sirt6-mediated Nrf2/HO-1 activation alleviates angiotensin II-induced DNA DSBs and apoptosis in podocytes, Food Funct. 12 (17) (2021) 7867–7882.
[56] Y. Zhang, Y. Kong, Y. Ma, S. Ni, T. Wikerholmen, K. Xi, et al., Loss of COPZ1 induces NCOA4 mediated autophagy and ferroptosis in glioblastoma cell lines, Oncogene 40 (8) (2021) 1425–1439.
[57] Y. Tian, J. Lu, X. Hao, H. Li, G. Zhang, X. Liu, et al., FTH1 inhibits ferroptosis through ferritinophagy in the 6-OHDA model of Parkinson's disease, NeuroTherapeutics 17 (4) (2020) 1796–1812.
[58] P. Wongprayoon, P. Govitrapong, Melatonin receptor as a drug target for neuroprotection, Curr. Mol. Pharmacol. 14 (2) (2021) 150–164.
[59] K. Shinozuka, M. Staples, C.V. Borlongan, Melatonin-based therapeutics for neuroprotection in stroke, Int. J. Mol. Sci. 14 (5) (2013) 8924–8947.
[60] M. Owczarz, J. Połosak, A. Domaszewska-Szostek, P. Kołodziej, A. Kuryłowicz, M. Puzianowska-Kuźnicka, Age-related epigenetic drift deregulates SIRT6 expression and affects its downstream genes in human peripheral blood mononuclear cells, Epigenetics 15 (12) (2020) 1336–1347.